FEMS Microbiology Ecology, 2023, **99**, 1–12
DOI: 10.1093/femsec/fiad013
Advance access publication date: 1 February 2023
Research Article

Microbial iron cycling is prevalent in water-logged Alaskan Arctic tundra habitats, but sensitive to disturbance

Alexander B. Michaud*, Rémi O. Massé, David Emerson

Bigelow Laboratory for Ocean Sciences, East Boothbay, ME 04544, United States
*Corresponding author. Bigelow Laboratory for Ocean Sciences, 60 Bigelow Dr., East Boothbay, ME, 04544, USA. Tel: +207-315-2567×411; E-mail: amichaud@bigelow.org
Editor: [Max Haggblom]

Abstract

Water logged habitats in continuous permafrost regions provide extensive oxic-anoxic interface habitats for iron cycling. The iron cycle interacts with the methane and phosphorus cycles, and is an important part of tundra biogeochemistry. Our objective was to characterize microbial communities associated with the iron cycle within natural and disturbed habitats of the Alaskan Arctic tundra. We sampled aquatic habitats within natural, undisturbed and anthropogenically disturbed areas and sequenced the 16S rRNA gene to describe the microbial communities, then supported these results with process rate and geochemical measurements. Undisturbed habitats have microbial communities that are significantly different than disturbed habitats. Microbial taxa known to participate in the iron and methane cycles are significantly associated with natural habitats, whereas they are not significantly associated with disturbed sites. Undisturbed habitats have significantly higher extractable iron and are more acidic than disturbed habitats sampled. Iron reduction is not measurable in disturbed aquatic habitats and is not stimulated by the addition of biogenic iron mats. Our study highlights the prevalence of Fe-cycling in undisturbed water-logged habitats, and demonstrates that anthropogenic disturbance of the tundra, due to legacy gravel mining, alters the microbiology of aquatic habitats and disrupts important biogeochemical cycles in the Arctic tundra.

Keywords: arctic, disturbance, gallionellaceae, geobacter, iron-oxidation, iron-reduction

Introduction

Microorganisms in the thawing active layer of Arctic permafrost habitats are responsible for the transformation and fate of thawed organic carbon and nutrients (Blaud et al. 2015, Faucherre et al. 2018). However, which microorganisms respire the thawed organic carbon matters for understanding the consequences of permafrost thaw on climate warming feedbacks, as the carbon can be converted to CO_2 or CH_4. Water-logged habitats of the tundra are one such location where thawed organic carbon could become CO_2 or CH_4 based on the microbial community and geochemical properties (Lipson et al. 2013, Herndon et al. 2015, Miller et al. 2015, Philben et al. 2020). These water-logged habitats also permit extensive redox interfaces where redox-active metals, such as Fe, can be microbially oxidized and reduced. The cycling of Fe in water-logged tundra habitats are potential hotspots for respiration of permafrost carbon, released during thaw, to become CO_2 or CH_4 (Miller et al. 2015, Philben et al. 2020, Patzner et al. 2022).

Microbial respiration of soil carbon from the tundra may be partially offset by uptake through increases in plant biomass; however, these plant biomass increases may be buffered by the availability of limiting nutrients. This balance between respiratory carbon losses and greater carbon uptake by plants is dependent on the bottom-up controls on nutrient availability. For example, the iron cycle exerts an influence on the phosphorus cycle through its ability to bind and release phosphorus (Herndon et al. 2019). Fe(III)-oxides bind and trap phosphorus based on the physical characteristics of the Fe(III)-oxides, with ferrihydrite-like Fe(III)-oxides having the ability to adsorb larger quantities of phosphate. Dissolution of the Fe(III)-oxides can release the phosphorus back into solution to be used by tundra plants. Thus, the redox state and microbial processes involved in iron cycling are significant for phosphorus mobility in the Arctic tundra.

Iron-reducing bacteria (FeRB) play an important role in remineralization of organic carbon within the Arctic tundra (Lipson et al. 2013, Megonigal et al. 2014, Miller et al. 2015, Philben et al. 2020). The production ratio of carbon dioxide to methane from thawed organic matter is dependent on the competition for organic carbon between the FeRB and methanogenic archaea (Philben et al. 2020). When FeRB outcompete methanogens for organic carbon oxidation the CO_2: CH_4 is high, with less warming potential (Myhre et al. 2013). In Fe(III)-poor habitats, the CO_2: CH_4 ratio is lower, promoting a larger warming potential from permafrost organic carbon remineralization (Miller et al. 2015). Competition for organic carbon between these two ecological groups of microorganisms is determined, in part, by Fe(III)-oxides, which serve as an electron acceptor for FeRB (Lovley and Phillips 1986). FeRB have a thermodynamic advantage over methanogenic archaea at circumneutral pH when the Fe(III)-oxides are present in the environment as nanoparticulate, poorly crystalline forms of Fe(III)-oxides (e.g. ferrihydrite) (Postma and Jakobsen 1996). Given the significant role of Fe(III)-oxides role in organic carbon rem-

Received: December 6, 2022. **Revised:** January 23, 2023. **Accepted:** January 31, 2023

ineralization and phosphorus binding potential, it is important to constrain the spatial distribution and rates of iron cycling within the tundra landscape.

Continuous permafrost environments within the North Slope of Arctic Alaska possess the physical features which allow iron-oxidizing bacteria (FeOB) to grow and produce Fe(III)-oxides. The shallow active layer is bounded by the perennially-frozen permafrost, which constrains most aqueous biogeochemical reactions during the thaw season (Neilson et al. 2018, Cochand et al. 2019). The end products from metabolic reactions mediated by plants and microorganisms remain in this active layer during the summer season and are not lost via advection to deep aquifers, as they can be in temperate latitudes or regions of discontinuous permafrost (Cochand et al. 2019). The shallow active layer is hydraulically active in the summer (O'Connor et al. 2019), which promotes rapid recycling of redox active elements. The oxidized layers are near the water table level or around submerged plants in moist acidic and non-acidic tundra, and wet sedge meadows (Zak and Kling 2006, Herndon et al. 2019). FeOB live at this oxic-anoxic interface in the Arctic tundra and gain energy from the oxidation of ferrous iron (Emerson et al. 2010, Emerson et al. 2015). In circumneutral aquatic habitats, FeOB produce insoluble, conspicuous, reddish-orange mats of Fe(III)-oxides (biogenic Fe mats) at the oxic-anoxic interface (Emerson et al. 2010). Given the shallow groundwater and short hydrological plow paths (O'Connor et al. 2019), favorable oxic-anoxic interfaces for FeOB could be abundant in continuous permafrost regions of the Arctic. These conditions that favor shallow active layer hydrology and favorable oxic-anoxic niches for FeOB are disappearing due to permafrost thaw. With the loss of FeOB habitat, less poorly crystalline Fe(III)-oxides are produced with unknown consequences for phosphorus mobility and organic carbon remineralization through iron reduction; however, little is known about the current ecology of iron cycling microorganisms from Arctic tundra.

The goals of the work presented here were to compare tundra habitat types which support biogenic Fe mats and contrast them to similar habitat types that lack Fe mats, and to determine if biogenic Fe mats support a unique community of microorganisms, geochemistry, and rates of iron reduction. We collected geochemical and biogenic Fe mat samples over the course of four weeks during summer from three different landscape habitat types (ponds, wet sedge meadows, and iron seeps) and conducted iron reduction assays from these habitat types. Samples were collected near Toolik Field Station on the North Slope of Alaska, USA.

Methods

Site description

The North Slope of Alaska is characterized by continuous permafrost with a shallow active layer that develops during the summer season (Shaver et al. 2014). Around the Toolik Lake Field Station (TFS), the interaction of soil age since last glaciation and topography create four unique terrestrial ecosystems. These ecosystems include moist acidic tussock, moist non-acidic tussock, heath, and wet sedge meadows (Fig. S1) (Shaver et al. 2014). Wet sedge meadows were the dominant ecosystem type which hosted visible biogenic Fe mats at the soil-water interface, thus all of our samples, except the low-iron sites, were within low-lying areas dominated by non-tussock forming sedges (e.g. *Carex* and *Eriophorum* species; (Boelman et al. 2003). In wet sedge meadows, *Eriophorum vaginatum* (Cotton grass) typically does not grow in the characteristic tussock morphology of a bunch or tuft. Wet sedge meadows are found in low-lying areas of the tundra, beyond hill toe slopes, and arecharacterized by standing water or slowly flowing surface water (Giblin et al. 1991). Biogenic Fe mats in wet sedge meadows were thin (0.5–2 cm) and flocculant, typically associated with submerged plant stems and leaves. Ponds were typically depressions within larger wet sedge meadows and varied in size from a few meters to tens of meters across, with < 2 m depth of standing water. Biogenic Fe mats in ponds were thin (~0.5 cm) coatings on the pond sediment/soil-water interface. Seeps were typically found near river banks with an abundance of thick (~10 cm) biogenic Fe mats. Our sampling took place in two distinct watersheds (Fig. 1). Six sampling sites were established in the Oksrukuyik Creek (OKS) watershed, representing four ponds, one wet sedge meadow, and a riverbank iron seep (Fig. 1). The other three ponds that contained biogenic Fe mats were depressions within the wet sedge meadow. The river bank seep was directly adjacent to the Oksrukuyik Creek and surrounded by non-tussock forming *Carex* and *Eriophorum* species.

Another eight sites were established within the Toolik Lake watershed, near the Toolik Lake inlet stream. Of these eight sites, four were ponds, two were wet sedge meadows, and one was an iron seep along the banks of the Toolik Lake Inlet stream.

In both watersheds, the low iron sites were ponds located within old gravel mining scars, except for one pond within the TFS watershed. These scars are not immediately recognizable, since they are now vegetated; however, the vegetation types are dominated by *Salix* species, which differs from the surrounding, undisturbed tundra. We used historical land use maps to determine that two of the low iron pond sites from the Toolik Lake watershed and one within the OKS watershed were located in previously disturbed sites that had been used for gravel mining during the construction of the Dalton Highway (Toolik Field Station, GIS), approximately 50 years ago. The third low iron pond in the Toolik Lake watershed was primarily a mat composed of benthic diatom species with no visible FeOB sheaths or stalks as confirmed by microscopy.

Sample collection

We visited all sample sites (Fig. 1; Table S1, Fig. S1) between 19 June 2019 and 20 July 2019. We collected 4 to 6 samples for microbial community composition, methane, dissolved oxygen, and pH at each site over this one-month period. Extractable Fe samples were collected 1 to 4 times from each site during these sampling visits over the one-month period. Samples for microbial community analysis, Fe-extractions, and Fe-reduction assays included sediment from the surface 1 cm of the sediment-water interface (pond sites) and biogenic Fe mat from the soil-water interface (seep and wet sedge meadow sites). A YSI ProPlus water quality meter was used to measure the temperature, conductivity, pH, and dissolved oxygen of the water above the biogenic Fe mats before sampling began. The pH and dissolved oxygen probes were calibrated weekly using a three-point calibration curve with pH 4, 7, and 10 buffers and a two-point calibration using an ascorbic acid and NaOH solution for the 0% oxygen standard and humid air for the 100% oxygen standard. Dissolved methane samples were collected at each sampling by submerging a 30 ml glass serum vial into the overlying water at each site. The vial was filled without allowing the water to bubble into the vial. Once completely full, the vial was capped with a blue butyl-rubber stopper that had a 21 ga needle through it to allow displaced water to escape, while ensuring a bubble-free headspace. Then, 100 μL of 10 M NaOH was injected with a syringe and needle with displaced water exit-

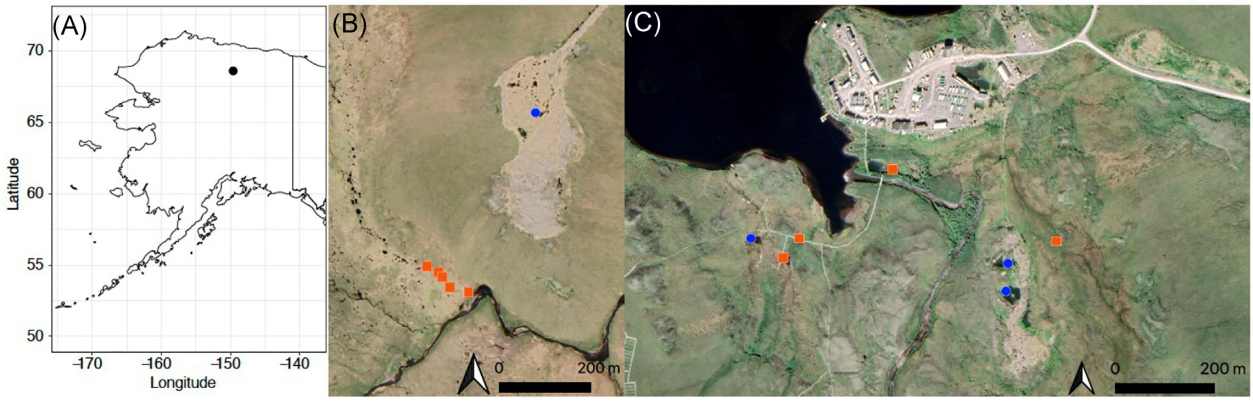

Figure 1. Map of Alaska, USA, with the Toolik Lake Field station area indicated with the black dot **(A)**, and highlighting the aerial imagery with study site locations for those in the OKS watershed **(B)** and Toolik Lake watershed **(C)**. Red squares indicate high Fe sites and blue circles indicate low Fe sites. Panel B and C map data: Google, Maxar Technologies.

ing through the vent needle. The needles were immediately removed and an Al crimp cap was used to seal the butyl-rubber stopper in place. Samples from ponds, wet sedge meadows, and seeps for microbiological analysis were collected at the soil water interface with a sterile 25 ml serological pipette and a battery powered pipette hand pump. The samples were transferred into sterile 15 ml conical centrifuge tubes and stored on blue ice until returning to the laboratory at TFS. A small amount of biogenic Fe mat material was removed before further sample processing and a wet mount of the material was imaged under phase contrast microscopy at 20X to 40X magnification. The samples were allowed to settle for ~1 h at 4°C after returning to the laboratory, then excess water was decanted until ~5 ml of liquid remained and tubes could be safely frozen at −20°C to avoid cracking. Replicate tubes were collected in this manner for DNA and Fe extraction. Samples were shipped on blue ice (methane) or frozen (DNA and Fe extraction) to Bigelow Laboratory for Ocean Sciences and stored at 4°C (methane) or frozen at −80°C (DNA and Fe extraction) until further analysis.

Geochemical sample processing

Sequential Fe extractions were conducted using a standard method (Laufer et al. 2020), but modified to accommodate handling of the flocculant biogenic Fe mats. Extraction material was added to a pre-weighed 0.2 μm spin filter cartridge. These spin filter cartridges were centrifuged for 15 min at 10 000 × *g* to yield a standardized dewatered wet weight of sediment or biogenic Fe mats on the spin filter cartridge. Due to the high quantity of iron in some of these samples, we did not want to use the standard oven-dried method before extracting iron, as this process would alter the crystallinity and potentially the valence state of the iron and thus the amounts of Fe(III) and Fe(II) extractable in the sequential iron extraction method (Zhang et al. 2001). The spin filter cartridge was transferred to a 15 ml conical centrifuge tube and 5 ml of 0.5 M HCl was added to each tube and vortexed to mix. The extraction was run for 1 h at 20°C in the dark on a shaker table set at 60 RPM. After the incubation period, 1 ml of extraction solution was filtered through a 0.2 μm PTFE syringe filter and collected in a clean microcentrifuge tube. Filtered 0.5 M HCl extraction solutions were diluted 1 : 10 with 1 M HCl and stored at 4°C until quantification. The extraction vials were then centrifuged at 5000 x g for 15 min to pellet the undissolved biogenic Fe mat or sediment. The 0.5 M HCl extraction solution was pipetted off, then 5 ml of anoxic 6 M HCl was added to the vial to begin the second step in the sequential extraction. The vial was vortexed and the entire contents of the centrifuge tube were transferred to a glass vacutainer with a septa-containing lid. The 6 M HCl extraction was incubated in a dark, 70°C water bath for 24 h and mixed three times throughout the incubation. After the incubation, the vials were decapped and 1 ml of extraction solution was filtered through a 0.2 μm PTFE syringe filter and collected in a clean microcentrifuge tube. The filtered 6 M HCl extraction solutions were immediately diluted (1 : 6) with 1 M HCl for a 1 M final concentration to avoid the oxidation artefacts created by storing extracted Fe(II) in 6 M HCl (Porsch and Kappler 2011). Fe(II) and total Fe in the filtered extraction solutions were quantified using the ferrozine method with the 10% hydroxylamine hydrochloride step within 24 h of ending the extraction (Stookey 1970). Both the 0.5 M and 6 M HCl solutions were bubbled with N_2 for 10 min before use to drive off any dissolved oxygen. The Fe(III) was quantified by subtracting Fe(II) from the total Fe (Laufer et al. 2020). All sample handling steps were conducted in a N_2-flushed portable glove bag.

The dissolved methane concentration was determined by the headspace equilibrium method (Magen et al. 2014). A gas-tight syringe fitted with a three-way valve was prepared by flushing the syringe three times with methane-free (below detection limit; <0.1 ppm) N_2 gas and on the final flush 12 ml was drawn into the syringe, a needle was attached, and 2 ml of methane-free N_2 was pushed out to flush the three-way valve and needle dead space. The gastight syringe needle was then immediately inserted through the stopper. We added 10 ml of methane-free N_2 gas to each vial and allowed the N_2 gas to displace 10 ml of sample water, which was collected through a needle into a 10 ml syringe. Then, the collection syringe was removed and the gastight syringe was used to inject an additional 10 ml of methane-free N_2 into the headspace to produce a 2 atm overpressure in the headspace. The vials were shaken vigorously for 2 min and stored upside down for 2 h at room temperature. Then, 1.5 ml of headspace gas was removed with a N_2-flushed needle and syringe (Magen et al. 2014). The 0.5 ml of sample was used to flush needle volume, then 1 ml was immediately injected into a gas chromatograph equipped with a flame ionization detector (SRI 310C). The temperature and atmospheric pressure of the room was recorded at each injection. Sample peak areas were quantified using a four-point standard curve using a certified 100 ppm CH_4 standard.

DNA extraction, sequencing, processing, and analysis

Biogenic Fe mat samples were removed from the freezer and allowed to thaw at room temperature. Once thawed, the samples were centrifuged at 1500 × *g* for 5 min at 10°C to loosely pellet the material. The overlying water was decanted until only the pellet remained. DNA was extracted using a DNeasy power soil kit (Qiagen). A sterile, cutoff 1 ml pipette tip was used to pipette 0.25 ml of Fe mat pellet into a bead-beating tube with 200 μl of bead-beating solution removed. Then, 200 μl of phenol-chloroform-isoamyl alcohol (PCI; 25 : 24 : 1, VWR Life Sciences) was added to the bead beating tube, as we have found this improves DNA recovery from iron-rich mineral samples (Emerson et al. 2015, Scott et al. 2015). After the PCI step, the manufacturers protocol was followed. Bead beating was conducted for 10 min at 20 Hz. DNA was eluted from the silica member filter with 75 μl of molecular-grade water and stored frozen at −80°C. DNA was sent to Integrated Microbial Resources (Dalhousie University) for Illumina MiSeq paired-end sequencing of 300 bp (using version 3 chemistry) of the V4V5 variable region of the 16S rRNA gene, using the 515F/926R primer pair (Parada et al. 2016). Raw sequences were assembled, then quality controlled, clustered, and classified using the 16S rRNA gene amplicon processing software, mothur (Schloss et al. 2009). Quality sequences include those that do not contain ambiguous bases, homopolymers longer than 8 nt, or are longer or shorter than the length expected for the primer pair and were discarded. Vsearch (v2.13.3) was used to detect chimeric sequences (Rognes et al. 2016). These chimeric sequences were removed. All samples were subsampled to the lowest number of sequencing reads (n = 16 035) of the samples within this data set. Clustering of operational taxonomic units (OTU) was done at the 97% similarity level. The SILVA database v.138 (release date 16 Dec 2019) was used for taxonomic assignment of each OTU (Quast et al. 2013).

DNA sequence processing

Analysis of OTU and taxonomy table outputs from mothur (Kozich et al. 2013) was conducted in R using packages ggplot2 and tidyverse (Wickham et al. 2019, R Core Team 2020). Statistical analyses of microbial communities and geochemical parameters were conducted using labdsv, vegan, indicspecies, rstatix, and datarium (Roberts 2007, Cáceres and Legendre 2009, Oksanen et al. 2013, Kassambara 2021a and 2021b). In particular, the anosim function within the vegan package was used to test the similarity of high and low Fe site communities and high Fe communities in ponds, wet sedge meadows, and seeps. The comparison of microbial communities from high and low Fe sites indirectly tests the differences between natural and disturbed tundra sampling sites. The non-metric multidimensional scaling analysis was performed with the metaMDS function and environmental variable vectors were calculated with the envfit function, both within the vegan package. The indicator species analysis was performed using the multipatt function within the indicspecies package. We discarded OTUs that had ≤10 reads total from all sample sites. These sequence data are deposited in the NCBI sequence read archive under Bioproject (PRJNA769663) accession numbers (SAMN22158831–SAMN22158899).

Iron reduction assay

Biogenic Fe mat samples were collected from the soil-water interface of high Fe pond and wet sedge sites and a low Fe pond within both the Toolik Lake and OKS watersheds. Overlying water (2 L) from each of these sites was also collected. All samples were transported back to the lab in a cooler at 4°C. The biogenic Fe-mat samples were centrifuged at 500 × *g* for 5 min to pellet soil-water interface material. Then, ∼2 g of material from each site was placed in a glass serum vial and 20 ml of water collected at the respective site was added to the serum vial and amended with a sterile sodium citrate solution to 10 mM final concentration. The citrate solution was added to bind the Fe^{2+} released during dissimilatory iron reduction (Laufer et al. 2020). Following these additions, the soil-water slurry in each vial was bubbled with N_2 for 5 min with an inline 0.2 μm filter before the vials were capped with a butyl rubber stopper and Al crimp sealed. Four incubation vials were made for each high Fe site, three live and one killed-control vials. The two low Fe sites had two sets of three live and one killed-control vials; to one set we added 200 μl of centrifuge-concentrated biogenic Fe mat. The killed-control vials were all treated by boiling the sealed vial for 10 min. For all vials, The Fe^{2+} concentration was determined by sampling every 12 h for 4 d. Fe^{2+} samples were collected with a N_2-flushed needle and syringe; the 300 μL sample for Fe^{2+} was passed through a 13 mm 0.2 μm pore size nylon filter into a clean 1.5 ml tube, and 100 μl of filtered water was pipetted immediately into 1 ml of 1 M HCl to fix the Fe^{2+}. The ferrozine assay described above was used to quantify Fe^{2+} concentration.

Results

Geochemistry

The sequential HCl Fe extraction data helped to delineate between high and low Fe sites in addition to visible flocculant Fe mats at the sediment-water interface of ponds or clinging to submerged plant stems and leaves in wet sedge meadows. These high Fe sites always contained ≥59 μmol Fe(III) gdw^{-1} of total extractable Fe(III) (0.5 M + 6 M HCl extraction fractions). The low Fe sites always contained ≤20 μmol Fe(III) gdw^{-1} of total extractable Fe(III) (Fig. 2A). The high Fe sites contained significantly ($P < 0.001$) more total extractable Fe(III) compared to ponds that were classified as low Fe sites (Fig. 2A). Methane concentrations showed higher variability, and were at the higher end of the concentration range within the high Fe sites compared to low Fe sites, but there was no statistically significant difference in overall methane concentration of water collected from high and low Fe sites (Fig. 2B). The pH of water from all low Fe sites and timepoints (mean: 8.5; range: 7.3–9.6) was significantly higher than that from all high Fe sites and timepoints (mean: 6.9; range: 6.4–7.9) (Fig. 2C). Ponds had the highest mean temperatures (13.7°C) of the three habitat types sampled, followed by wet sedge meadow sites (11.5°C) and seeps (6.6°C) (Table S1). Dissolved oxygen in the overlying water of sampled sites always remained below 395 μM, with time points earlier in the summer typically having higher concentrations than later in the year. High Fe sites were more likely to have oxygen concentrations that decreased to hypoxic levels near ∼100 μM. Seep and wet sedge meadows sites routinely had oxygen concentration <20 μM (Table S1).

Microbial community analysis

The alpha diversity was significantly higher ($P < 0.005$) in the low Fe sites than in the high Fe sites (Fig. 3A). The OTU compositions of high Fe and low Fe sites were significantly different and the variation between the groups is much greater than the variation within the groups (ANOSIM: $P < 0.001$; ANOSIM R statistic = 0.8559). Within the high Fe sites, OTU compositions and alpha diversity from samples collected from the three habitat types (ponds, wet

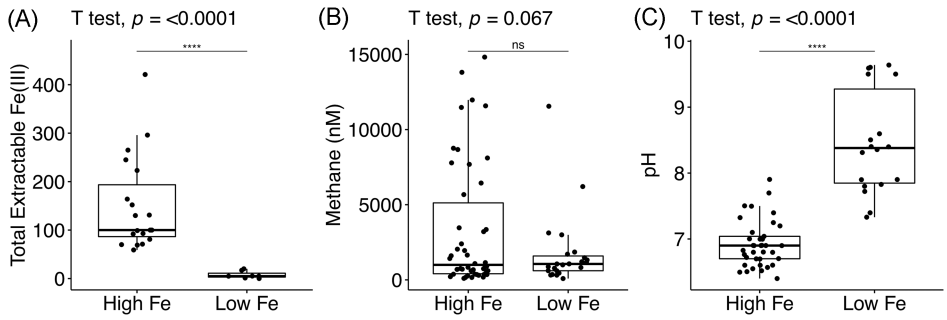

Figure 2. The total extractable Fe(III) **(A)**, methane **(B)**, and pH **(C)** of high and low Fe sample sites with results of the t-test displayed above each plot.

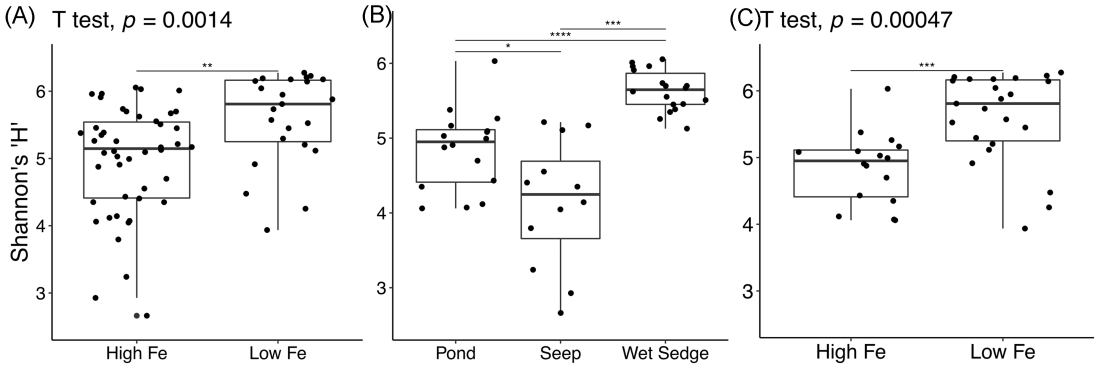

Figure 3. Alpha diversity statistics for all high and low Fe sites **(A)**, high Fe sites based on the feature type **(B)**, and high and low Fe ponds only **(C)**. Asterisks indicate significance codes of T-test, where $* = P < 0.01$ and **, ***, **** are all $P < 0.005$.

sedge meadows, and seeps) show significant differences (alpha diversity; all pairwise comparisons $P < 0.005$; Fig. 3B), but there was higher similarity within the habitat groups, showing more overlap of OTUs between groups (ANOSIM: $P < 0.001$; ANOSIM R statistic = 0.5029) than the OTU similarities between high and low Fe sites. Low Fe ponds have significantly greater alpha diversity compared to high Fe ponds ($P < 0.005$; Fig. 3C). These between group differences are shown within the NMDS ordination (Fig. 4) and illustrates the high and low Fe sites separated along NMDS axis 1, while the high Fe sites are separated along NMDS axis 2. The overall stress of the NMDS plot was 0.132. The environmental vectors are plotted on top of the microbial community composition points, but only the pH vector shows strong ($r^2 > 0.6$) and significant ($P < 0.01$) correlations to the ordination patterns of the microbial communities. The iron extraction data from all sampled sites (0.5 M HCl extractable Fe(III), and 6 M HCl extractable Fe(III)) show significant ($P < 0.05$), but weak ($r^2 = 0.32$) correlations to the ordination patterns of the microbial communities. It appears that the high Fe sites are separated along the methane and oxygen concentrations vectors, but these vectors are not significant ($P > 0.05$) and weak correlations ($r^2 < 0.2$) to the ordination patterns of the microbial communities seen (Oksanen et al. 2013).

High Fe sites contained 36 unique OTUs that were greater than 0.1% relative abundance, had an indicator species stat value of greater than 0.5, and were statistically significant ($P < 0.01$) to be found more often in high Fe sites (Fig. 5). These OTUs comprised 24 unique, named families. Most notably, families containing microorganisms known to be active in the iron cycle (*Gallionellaceae*, *Comamonadaceae*, *Geobacteraceae*) and methane oxidation (*Methylomonadaceae*, *Methanobacteriaceae*, *Methylophilaceae*). Low Fe sites contained 54 unique OTUs that were greater than 0.1% relative abundance, had an indicator species stat value of greater than 0.5, and were statistically significant ($P < 0.01$) to be found more often in low Fe sites (Fig. 5). These OTUs comprised 36 unique, named families. Most notably, families containing cyanobacteria (*Nostocaceae*) and heterotrophic bacteria (*Sphingomonadaceae*, *Xanthomonadaceae*). The *Comamonadaceae* family was the only family to have OTUs represent indicator species for both high and low Fe sites; however, while the family was represented in both high and low Fe sites, the indicator OTU identified to the genus level as *Rhodoferax* was only present in the high Fe sites. The high and low Fe sites did not share the same *Comamonadaceae* indicative OTUs.

Iron-oxidizing bacteria were grouped together and included members of the *Gallionellaceae* family and *Leptothrix* genus for the purposes of summing the different groups of FeOB present in biogenic Fe mats (Table S2). The *Gallionellaceae* have a mean relative abundance of 2.6% in high Fe sites, but 0.03% in low Fe sites (Fig. 6), and *Sideroxydans* was the most abundant member of the *Gallionellaceae* family across all habitat types sampled (Fig. 6). FeOB members of the *Leptothrix* genus were present in high and low Fe sites at roughly equal abundance, with mean relative abundances of 0.5% and 0.9%, respectively (Fig. 6). All identified FeRB (Table S2) were more abundant in the high Fe sites with a mean relative abundance of 4.2% and 1.1% in low Fe sites. Members of the *Geobacter* genus were the most abundant FeRB detected in the high Fe sites, with *Geothrix*, *Aneromyxobacter*, *Citrifermentans*, and *Desulfuromonas* present as well, but at lower relative abundances (Fig. S1). Other putative FeRB taxa are present as the most abundant OTU and related to *Rhodoferax*, which is part of the most abundant family (*Comamonadaceae*) found in this study (Fig S2). High Fe pond sites typically had the highest relative abundance across all FeRB genera, except for OTUs within the *Desulfuromonas* that were highest in the seep habitat type (Fig. S2B). The methane-

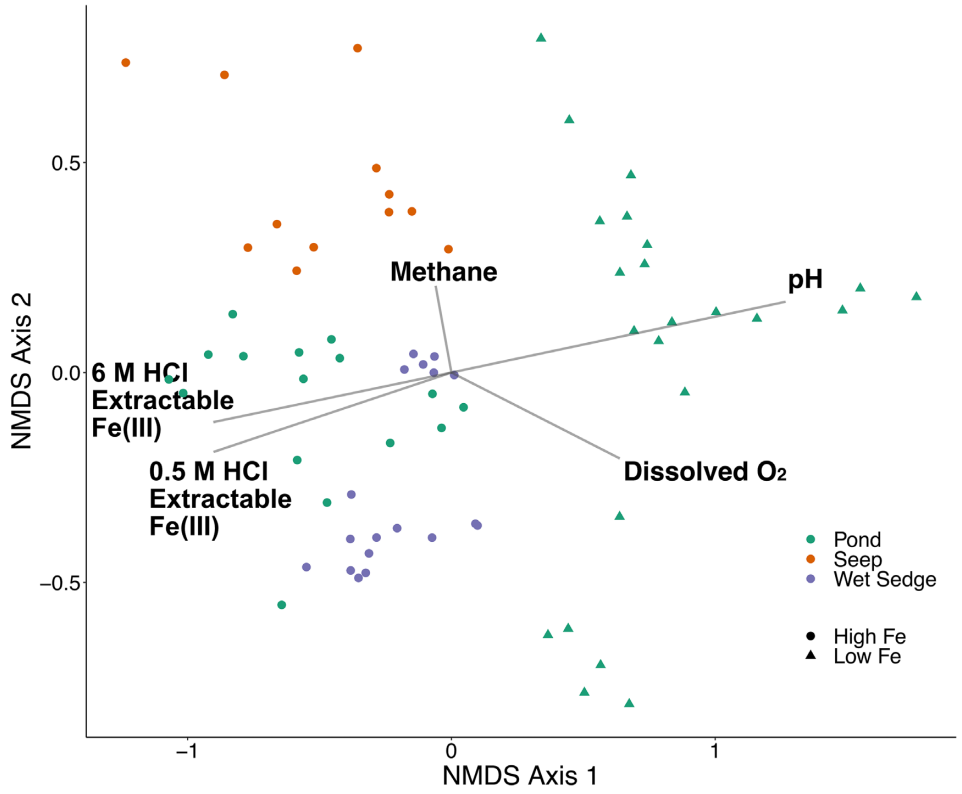

Figure 4. An NMDS plot of high and low Fe sites (circles and triangles) and pond, seep, and wet sedge feature types (green, orange, purple). The overall stress of the NMDS was 0.132.

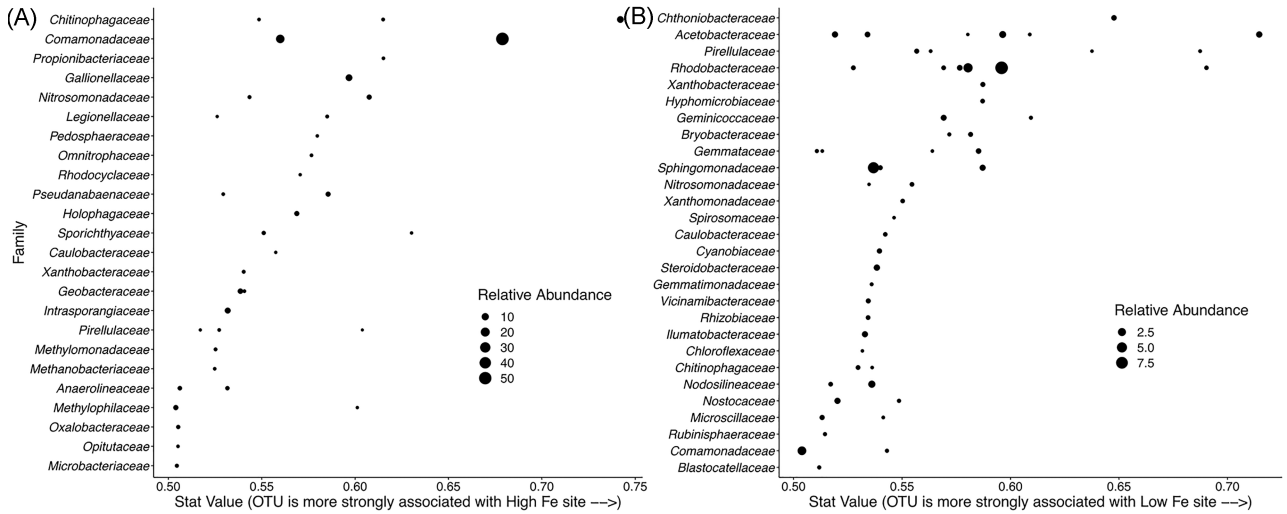

Figure 5. OTUs (black dots) within named families that are indicative of high Fe sites **(A)** and low Fe sites **(B)** with a stat value that is >0.5, significant ($P < 0.001$), and a relative abundance > 1%. Families with multiple dots indicate more than one OTU within that family was identified as indicative of high or low Fe site. The higher the stat value, the stronger the association of that OTU with the respective high or low Fe conditions.

oxidizing taxa (Table S2) had a higher mean relative abundance in high Fe sites (3%) compared to low Fe sites (1.1%) (Fig. 6D), with members of the *Methylomonadaceae* having the highest relative abundance of the detected methane-oxidizing families (Fig. S2C).

Iron reduction assays

Iron reduction was measurable at all high Fe sites (Table 1, Fig. 7). Pond and wet sedge sites from the TFS watershed had the same pattern with a ~60 h lag period (0.063 to 0.074 μmol Fe^{2+} gdw^{-1}) that then increased into a growth phase (0.25 μmol Fe^{2+} gdw^{-1}). The OKS sites did not have a lag period, and the pond site did show higher rates of iron reduction (0.23 μmol Fe^{2+} gdw^{-1}) than the wet sedge site (0.1 μmol Fe^{2+} gdw^{-1}). The low Fe sites always had near zero rates of iron reduction (<0.015 μmol Fe^{2+} gdw^{-1}), even when excess biogenic mat was added. The killed controls always also had near-zero rates of iron reduction (<0.02 μmol Fe^{2+} gdw^{-1}).

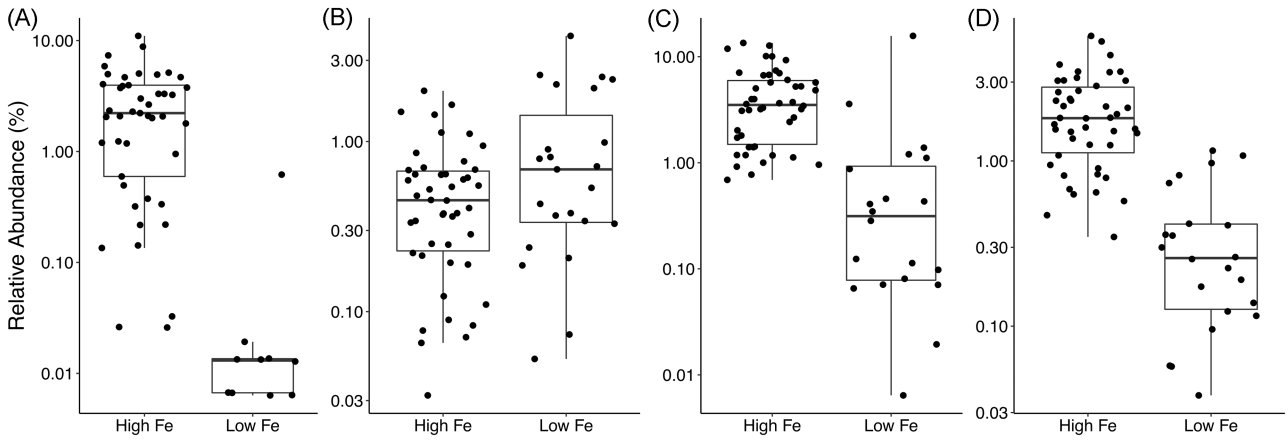

Figure 6. Relative abundances of *Gallionellaceae* **(A)**, *Leptothrix* **(B)**, iron-reducing bacteria **(C)**, and methylotrophic **(D)** taxa found in high and low Fe sample sites.

Table 1. Linear model details and statistics for iron reduction assays.

	Fe	Feature	Addition	Live/Kill	Slope (μmol Fe^{2+} gdw^{-1} d^{-1})		R^2		*P* value	
					Lag	Growth	Lag	Growth	Lag	Growth
TFS	High	Pond	None	Live	1.5	6.0	0.56	0.87	<0.01	<0.01
				Kill	0.46		0.46		0.26	
		Wet sedge		Live	1.8	6.0	0.57	0.88	<0.01	<0.01
				Kill	0.20		0.38		0.35	
	Low	Pond	None	Live	0.026	0.26	0.88	0.78	<0.01	<0.01
				Kill	0.029		0.61		0.11	
				Live	0.036	0.36	0.88	0.83	<0.01	<0.01
			BiogenicFe							
				Kill	0.018		0.61		0.11	
OKS	High	Pond	None	Live	5.5		0.93		<0.01	
				Kill	−0.65		0.97		<0.01	
		Wet sedge		Live	2.4		0.94		<0.01	
				Kill	0.013		0.055		0.9	
	Low	Pond	None	Live	0.20		0.89		<0.01	
				Kill	0.0020		0.09		0.84	
				Live	0.24		0.83		<0.01	
			BiogenicFe							
				Kill	0.0020		0.12		0.78	

Discussion

Role of iron-oxidization and iron-reduction arctic fe-rich habitats

High Fe sites on the North Slope of AK are defined here by a visible, reddish-orange ferric iron microbial mat. These mats were especially abundant in low-lying, water-logged areas of the tundra dominated by non-tussock-forming sedges (*Carex* and *Eriophorum* species, wet sedge meadows), commonly referred to as wet sedge meadows. Among our study focal areas, the high Fe sites were inhabited by known FeOB from the family *Gallionellaceae* and genus *Leptothrix* (Family *Commamonadaceae*) (Fig. 5 and Figs S2 and S3).

The primary component of these extracellular structures are poorly crystalline Fe(III)-oxides, primarily of the mineral ferrihydrite (Chan et al. 2009, Vigliaturo et al. 2020). Sheaths and stalks, commonly produced by *Leptothrix* spp. and *Gallionella* spp., were observed at most, but not all of the high Fe sites (Figs S5 and S6). These FeOB are the primary builders of the biogenic Fe mats found throughout our sampling sites; however, their relative abundance and distribution does vary based on sample site type (Fig. 6; Fig. S2). OTUs related to the genus *Leptothrix* are found in equal relative abundance in high and low Fe sites, compared to the OTUs within the *Gallionellaceae* family which are found in greater relative abundance in high Fe sites only (Fig. 6). This differential abundance between these two groups of FeOB is consistent with recent evidence that *L. ochracea*, one of the most common sheath-forming FeOB, can grow mixotrophically (Fleming et al. 2018), and that other *Leptothix* species can grow as heterotrophs (Ghiorse 1984), while members of the *Gallionellaceae* family are strict chemolithoautotrophs, coupling the oxidation of ferrous iron to the reduction of oxygen for growth (Hallbeck and Pedersen 2015). OTUs related to *Leptothrix* were also found in greatest abundance in biogenic Fe mats within wet sedge meadows, where the biogenic Fe mats were associated with submerged plant stems and leaves (Fig. S2A). Wet sedge meadows may also favor the mixotrophic metabolism of *Leptothrix* due to root exudates and abundant decaying organic matter (Giblin et al. 1991, Shaver et al. 2014). Among the *Gallionellaceae* no discernible patterns of habitat preference were observed. We also did not observe successional patterns between the *Gallionellaceae* and *Leptothrix* related OTUs (Fig. S4) over the course

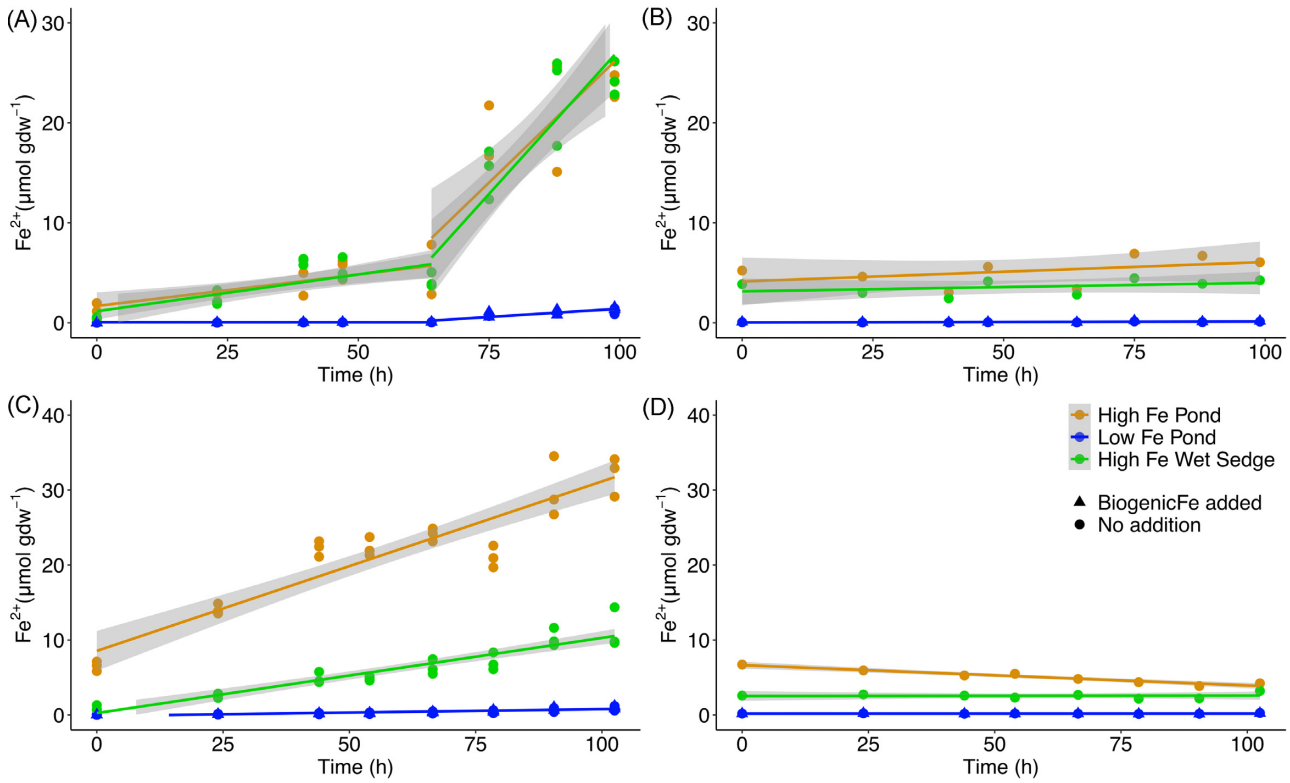

Figure 7. Time course plots of Fe^{2+} from live **(A, C)** and killed **(B, D)** treatments of sample sites within the TFS (A, B) and OKS (C, D) watersheds. Lines represent the linear models of Fe^{2+} over time with the grey shading indicating the 95% confidence interval for the linear model. High Fe sites within the TFS watershed had a ~60 h lag period and linear models were fit for both the lag and growth phases. The low Fe site blue triangles and circles are difficult to distinguish because the plot on top of each other.

of our observation period. Successional patterns have been observed in temperate, wetland-associated biogenic Fe mats that can transition from being dominated by the *Gallionellaceae* in early spring to *Leptothrix*-dominated biogenic Fe mats, later in the growing season (Fleming et al. 2014). Our 6-week study encompassed late spring to mid-summer which is concurrent with the greening phase of wet sedge meadow dominant plant species, *Eriophorum vaginatum*, which is similar to the spring-summer transition observed by Fleming et al. (2014) in a temperate ecosystem. These findings suggest that ecological patterns observed among temperate communities of Fe-cycling microbes may not hold in the Arctic, where a shallow active layer underlain by permafrost strongly influences hydrodynamic processes and source of Fe^{2+} for FeOB.

Iron-reducing bacteria (FeRB) were present in high abundance in many of the surficial sediments and biogenic Fe mats that we sampled (Figs S5, S6 and S2B). These FeRB taxa were primarily related to members of the genus *Geobacter*, which is a well-known genus of FeRB (Coates et al. 1996, Methé et al. 2003). OTUs related to other FeRB genera, such as *Geothrix* and *Anaeromyxobacter* (Wagner et al. 2017), were also detected within the biogenic Fe mats sampled from the three habitat types (Fig. S2B). The FeRB genera present in biogenic Fe mats around Toolik Field Station are less diverse compared to those found in active layer soils. For example, *Pelobacter*, *Shewanella*, and *Carboxydothermus* were not detected within the high Fe sites we sampled, but these genera were found in active layer soils of northern and western Alaska (Wagner et al. 2017). The high abundance (~1–10%) of FeRB within the biogenic Fe mats supports the idea that high Fe sites contain active Fe-cycling via organic carbon oxidation, coupling it to the reduction of ferric iron.

The results of the Fe-reducing experiment (Fig. 7) indicate that FeRB are active within the high Fe sites, consistent with their high relative abundance in 16S rRNA gene amplicon libraries (Fig. 6). This activity is also consistent with the high percentage (81 ± 16% [avg±SD]) of poorly-crystalline Fe(III)-oxides found in high Fe ponds and wet sedge meadow sites (Table S1). It is well established that biogenic Fe(III)-oxides produced by FeOB are thermodynamically favorable electron acceptors for dissimilatory Fe-reducers (Emerson and Revsbech 1994, Roden and Wetzel 1996), as fine-scale analysis shows that FeOB produce poorly crystalline extracellular Fe(III)-oxides, such as ferrihydrite (Chan et al. 2009, 2011, Vigliaturo et al. 2020). Further, the high percentage of 0.5 M HCl extractable Fe(III) was maintained over the course of the summer at our high Fe sites (Table S1), indicating that there was continual production of poorly-crystalline Fe(III) phases, potentially through sustained internal Fe-cycling coupled to mineralization of organic matter (Sobolev and Roden 2002, Roden et al. 2012) and supported by the high relative abundances of both FeOB and FeRB (Figs 5 and 6). Continual Fe(III)-oxide production by FeOB would counteract the ageing process of Fe(III)-oxides to those less thermodynamically-favorable for FeRB (i.e. ferrihydrite to goethite, Aeppli et al. 2019). Oxygen concentrations of water overlying biogenic Fe mats also varied over the course of the sampling period, showing the potential for these habitats to experience transient hypoxia and an increased potential for anoxic conditions conducive to iron reduction (Table S1). Thus, these Arctic biogenic Fe mats may be hotspots of organic carbon degradation via iron reduction due to internal iron cycling within suboxic and anoxic microsites or during changes in hydrology which drives anoxia throughout the biogenic Fe mats (Herndon et al. 2019).

Significant microbial iron-mat community members and biogeochemical implications

FeOB and FeRB are foundational members of biogenic Fe mats, in large part due to the copious production by FeOB of filamentous Fe-oxides that add physical structure to their habitat. In this sense, they may act as ecological engineers (Fleming et al. 2018), constructing mats that also harbor phylogenetically and functionally diverse microbial communities that play important roles in other element cycles. The FeOB and FeRB taxa discussed above are also represented by families (*Gallionellaceae* and *Geobacteracaea*) that are statistically significant as indicator taxa of the high Fe sites that we sampled. The most abundant and indicative family of high Fe sites was *Commamonadaceae*, particularly the genus *Rhodoferax*. The most abundant OTU was related to *Rhodoferax ferrireducens* (99.1%, based on V4V5 region of the 16S rRNA gene), a facultative organism known to couple Fe(III) reduction to anaerobic respiration on acetate or lactate (Finneran et al. 2003, Zhuang et al. 2011). A recent study reported on a novel *Rhodoferax* strain isolated in Japan that could also grow via Fe-oxidation (Kato and Ohkuma 2021). We isolated a strain closely related to *R. ferrireducens* from a 10^{-5} dilution enrichment for microaerophilic FeOB from the OKS seep site; however, upon further analysis this strain was capable of heterotrophic growth under very low nutrient conditions, and growth coupled to lithotrophic Fe-oxidation or respiratory Fe-reduction in this strain has not been confirmed (D. Emerson, unpublished data). The exact role of these abundant *Rhodoferax*-related OTUs in these iron mat communities remains to be elucidated.

Methylotrophic taxa (Table S2) are also significant and indicative community members of the high Fe sites (Figs 5 and 6), especially the families *Methylomonadaceae* and *Methylophilaceae* (Gammaproteobacteria) (Fig. 5). We use the term methylotrophic throughout to acknowledge that these taxa are capable of methane oxidation and, in some cases, the oxidation of other C_1 compounds including methanol (Chistoserdova et al. 2009). Coincident with the presence of these methylotrophs, methane was detected in the waters at all sites with a wide range of concentrations from ~200–13 000 nM (Table S1), thus methane was available to support methanotrophy. We are aware of only one study that specifically looked for the presence of methane-oxidizing bacteria in temperate biogenic Fe mats (Kato et al. 2012). The dominant, putative methane-oxidizers from that study were in the family *Methylococcaceae* (Gammaproteobacteria), also present in the arctic mats, but were less abundant and not a significant, indicative taxa of high Fe sites (Fig. 5; Fig. S2C). The most abundant and active methylotrophic bacteria found in tundra soil are primarily composed of members of the *Methylocystaceae* (Alphaproteobacteria) (Blaud et al. 2015), categorized as type II methanotrophs. Type II methylotrophs possess a high-affinity methane monooxygenase gene and can inhabit low methane environments (Knief 2015). Whereas, type I methanotrophs (Gammaproteobacteria) are known to possess low-affinity particulate methane monooxygenase enzymes meaning they are better adapted to higher methane environments. Finding methylotrophs which are known to possess type I methane monooxygenase gene is indicative that biogenic Fe mats are occurring in relatively methane-rich environments, and selecting for a different population of methylotrophs compared to tundra soils. The structural properties of actively growing filamentous FeOB within wet sedge meadows, ponds, and seeps result in a loosely consolidated microbial mat that provides a large and relatively fixed surface area for the attachment of other microbes, including methane oxidizers. In fact, studies of wet sedge meadows show a relatively consistent fraction of methane oxidized, indicating there is efficient methane oxidation in these habitats (Moosavi and Crill 1998). We postulate that biogenic Fe mats observed in the wet sedge meadows are a methane biofilter atop saturated, organic-rich soils within wet sedge meadows and provide a relatively consistent habitat, both spatially and temporally, that promote Gammaproteobacterial methylotrophic bacteria across wet sedge meadows, an abundant habitat type in the tundra (Britton 1966, Walker et al. 1989). Nonetheless, the consistent presence of methane combined with significant abundance of methylotrophs indicates that there is continual production and consumption of methane occurring in these habitats where Fe-cycling is a dominant process. This provides further evidence that an active Fe-cycle does not fully inhibit methane production, and consumption (Lipson et al. 2010, Miller et al. 2015); however, determining the degree to which active Fe-cycling may suppress methanogenesis remains an open question.

Disturbance microbial ecology

Low Fe sites supported different microbial communities compared to high Fe sites (Figs 4, 5, and 6). These low Fe sites that we sampled in the TFS region were some of the only consistently water-logged sites that we could find that did not support conspicuous biogenic Fe mats at the soil or sediment surface. Three of the four low Fe sites were located in areas where gravel mining had occurred during the construction of the Dalton Highway in the early 1970s. The gravel mining removed the organic soil layer to access the gravel-rich glacial till nearly 50 years ago (Auerbach et al. 1997), yet conditions which support iron cycling have not returned to the ponds in these disturbed sites. By comparison, the surficial sediment from low Fe pond sites had a significantly different microbial community (Fig. 4) with different taxa predominating and, aside from *Leptothrix*, a notable absence of presumptive FeOB (Figs 4 and 6). The overall microbial diversity was higher at the low Fe sites (Fig. 3) compared to the high Fe sites. These findings suggest that the conditions which promote the presence of Fe mats act as an important environmental filter that selects for particular microorganisms, especially those involved in Fe-cycling, and may reduce overall microbial diversity. The significant difference of the microbial community structure found at high and low Fe sites can be seen in the separation of the community along the first NMDA axis (Fig. 4). One environmental driver contributing to the microbial community differences between the high and low Fe sites is pH. We know that pH is a major driver of microbial community composition in the Arctic (Malard and Pearce 2018, Malard et al. 2019) and low Fe sites sampled in this study have a significantly higher pH than high Fe sites (Figs 2C and 4). The pH of the site water is a significant environmental variable driving these community differences (Fig. 4). The pH of the low Fe ponds may be significantly higher compared to surrounding tundra due to the acid buffering capacity of the calcium carbonate-rich gravels that were mined for road building (Auerbach et al. 1997). The gravel mining disturbance at our low Fe site may be contributing through a loss of habitat and to the maintenance of basic pH conditions that together no longer support biogenic Fe mats at the surface of pond sediments. We extend the impacts of gravel mining and construction-related disturbance to an alteration of the microbial communities that inhabit the surface sediment of ponds, which may alter the biogeochemical cycling of iron and, by association, alter the movement of plant limiting nutrients, such as phosphorus (Herndon et al. 2019).

In fact, our Fe reduction rate measurements show that low Fe sites have very little measureable Fe reduction occurring (Fig. 7, Table 1). We attempted to stimulate Fe reduction by introducing biogenic Fe mats to the low Fe site incubations as a source of thermodynamically favorable Fe(III) (Figs 7A and C). These treatments resulted in rates of Fe reduction that were indistinguishable from the low Fe site incubations without added biogenic Fe mats (Fig. 7, Table 1). The loss of biogenic Fe mats has the potential to disrupt nutrient movement between the sediment and water column of these ponds due to the ability of Fe(III)-oxides to bind phosphorus and trace metals in lake sediments and soils (Whalen and Cornwell 1985, Cornwell and Kipphut 1992, Herndon et al. 2019). Without biogenic Fe(III)-oxides present, phosphorus may bind to more crystalline forms of Fe(III) minerals or other non-Fe minerals (i.e. Ca) (Herndon et al. 2019). These mineral phases bind phosphorus to minerals which are not impacted by microbial driven redox cycles and reduce recycling of phosphorus back to the water column. Thus, iron reducing microorganisms may play an important role in recycling phosphorus through their reductive dissolution of Fe(III) minerals, which occurs more readily with poorly crystalline Fe(III)-oxides. Gravel mining creates aquatic habitats that possess different microbial communities to natural tundra ponds and alters the function from one that is more likely to recycle plant-limiting nutrients to one that is more likely to sequester those nutrients.

Conclusions

Microbial communities associated with biogenic Fe mats in Arctic Alaska are taxonomically and functionally unique compared to other tundra habitats, and host abundant taxa important for carbon and iron cycling, with the *Gallionellaceae* being the major lithotrophic group of FeOB. These communities were relatively stable, showing little spatial variation across different Arctic habitat types. FeRB are abundant and contribute to making biogenic Fe mats potential hot spots of organic carbon remineralization, likely outcompeting methanogenesis in this habitat with abundant, biogenic and labile Fe(III)-oxides. Further, biogenic Fe mats host methane-oxidizing microorganisms that consume methane before it is emitted to the atmosphere. These key functional groups of microorganisms are lost from sites subjected to gravel mining activities, even after 50 years. Biogeochemical cycles within a gravel mining-impacted site have also been disrupted, as iron cycling does not appear to be active in these disturbed tundra aquatic habitats. We conclude that biogenic Fe mats are a major component of wet sedge meadows and other water-logged habitats underlain with permafrost. In these natural tundra habitats, iron cycling is active and disturbed habitats are likely to lose their iron cycle and the beneficial methylotrophic and iron reducing taxa that promote methane oxidation and phosphorus recycling, respectively.

Acknowledgments

We thank the Toolik Field Station staff for support and logistics of this project. WB Bowden, NR Record, P Villard, and FW Sutor assisted with field season planning and sampling. We thank B Orcutt for use of the gas chromatograph.

Supplementary data

Supplementary data are available at FEMSEC online.

Conflicts of interest statement. None declared.

Funding

Funding for this project was provided by US National Science Foundation Division of Environmental Biology (Award #1754358 to DE). ROM was supported by the National Science Foundation for the Bigelow Laboratory REU program (NSF Grant OCE 1460861)—REU Site: Bigelow Laboratory for Ocean Sciences—Undergraduate Research Experience in the Gulf of Maine and the World Ocean.

References

Aeppli M, Vranic S, Kaegi R *et al.* Decreases in iron oxide reducibility during microbial reductive dissolution and transformation of ferrihydrite. *Environ Sci Technol* 2019;**53**:8736–46.

Auerbach NA, Walker MD, Walker DA. Effects of roadside disturbance on substrate and vegetation properties in Arctic Tundra. *Ecol Appl* 1997;**7**:218–35.

Blaud A, Lerch TZ, Phoenix GK *et al.* Arctic soil microbial diversity in a changing world. *Res Microbiol* 2015;**166**:796–813.

Boelman NT, Stieglitz M, Rueth HM *et al.* Response of NDVI, biomass, and ecosystem gas exchange to long-term warming and fertilization in wet sedge tundra. *Oecologia* 2003;**135**:414–21.

Britton ME. Vegetation of the arctic tundra. In: Hanson HP (ed.), *Arctic Biology*. Corvallis, Oregon: Oregon State University Press, 1966;67–130.

Cáceres M de, Legendre P. Associations between species and groups of sites: indices and statistical inference. *Ecology* 2009;**90**:3566–74.

Chan CS, Fakra SC, Edwards DC *et al.* Iron oxyhydroxide mineralization on microbial extracellular polysaccharides. *Geochim Cosmochim Acta* 2009;**73**:3807–18.

Chan CS, Fakra SC, Emerson D *et al.* Lithotrophic iron-oxidizing bacteria produce organic stalks to control mineral growth: implications for biosignature formation. *ISME J* 2011;**5**:717–27.

Chistoserdova L, Kalyuzhnaya MG, Lidstrom ME. The expanding world of methylotrophic metabolism. *Annu Rev Microbiol* 2009;**63**:477–99.

Coates JD, Phillips EJP, Lonergan DJ *et al.* Isolation of *geobacter* species from diverse sedimentary environments. 1996;**62**:1531–6.

Cochand M, Molson J, Lemieux JM. Groundwater hydrogeochemistry in permafrost regions. *Permafrost Periglacial Proces* 2019;**30**:90–103.

Cornwell JC, Kipphut GW. Biogeochemistry of manganese- and iron-rich sediments in Toolik Lake, Alaska. *Hydrobiologia* 1992;**240**:45–59.

Emerson D, Fleming EJ, McBeth JM. Iron-oxidizing bacteria: an environmental and genomic perspective. *Annu Rev Microbiol* 2010;**64**:561–83.

Emerson D, Revsbech NP. Investigation of an iron-oxidizing microbial mat community located near Aarhus, Denmark: laboratory studies. *Appl Environ Microbiol* 1994;**60**:4032–8.

Emerson D, Scott JJ, Benes J *et al.* Microbial iron oxidation in the arctic tundra and its implications for biogeochemical cycling. *Appl Environ Microbiol* 2015;**81**:8066–75.

Faucherre S, Jørgensen CJ, Blok D *et al.* Short and long-term controls on active layer and permafrost carbon turnover across the Arctic. *J Geophys Res: Biogeosci* 2018;**123**:372–90.

Finneran KT, Johnsen C V., Lovley DR. Rhodoferax ferrireducens sp. Nov., a psychrotolerant, facultatively anaerobic bacterium that oxidizes acetate with the reduction of Fe(III). *Int J Syst Evol Microbiol* 2003;**53**:669–73.

Fleming EJ, Cetinić I, Chan CS *et al.* Ecological succession among iron-oxidizing bacteria. *ISME J* 2014;**8**:804–15.

Fleming EJ, Woyke T, Donatello RA *et al.* Insights into the fundamental physiology of the uncultured Fe-oxidizing bacterium leptothrix ochracea. *Appl Environ Microbiol* 2018;**84**: e02239–17.

Ghiorse WC. Biology of iron- and manganese-depositing bacteria. *Annu Rev Microbiol* 1984;**38**:515–50.

Giblin AE, Nadelhoffer KJ, Shaver GR *et al.* Biogeochemical diversity along a riverside toposequence in Arctic Alaska author. *Ecolog Monogr* 1991;**61**:415–35.

Hallbeck LE, Pedersen K. Gallionella. In: Whitman WB (ed), *Bergey's Manual of Systematics of Archaea and Bacteria*. Hoboken, New Jersey: John Wiley & Sons, Inc., 2015, 1–10.

Herndon EM, Kinsman-Costello L, Duroe KA *et al.* Iron (Oxy-hydr)oxides serve as phosphate traps in Tundra and boreal peat soils. *J Geophys Res: Biogeosci* 2019;**124**:227–46.

Herndon EM, Yang Z, Bargar J *et al.* Geochemical drivers of organic matter decomposition in arctic tundra soils author(s): *Biogeochemistry* 2015;**126**:397–414.

Kassambara A. rstatix. *Rstatix* 2021a.

Kassambara A. datarium. 2021b.

Kato S, Kikuchi S, Kashiwabara T *et al.* Prokaryotic abundance and community composition in a freshwater iron-rich microbial mat at circumneutral pH. *Geomicrobiol J* 2012;**29**:896–905.

Kato S, Ohkuma M. A single bacterium capable of oxidation and reduction of iron at circumneutral pH. *Microbiol Spectr* 2021;**9**, DOI: 10.1128/spectrum.00161-21.

Knief C. Diversity and habitat preferences of cultivated and uncultivated aerobic methanotrophic bacteria evaluated based on pmoA as molecular marker. *Front Microbiol* 2015;**6**:1346.

Kozich JJ, Westcott SL, Baxter NT *et al.* Development of a dual-index sequencing strategy and curation pipeline for analyzing amplicon sequence data on the miseq illumina sequencing platform. *Appl Environ Microbiol* 2013;**79**:5112–20.

Laufer K, Michaud AB, Røy H *et al.* Reactivity of iron minerals in the seabed toward microbial reduction – a comparison of different extraction techniques. *Geomicrobiol J* 2020;**37**:170–89.

Lipson DA, Jha M, Raab TK *et al.* Reduction of iron (III) and humic substances plays a major role in anaerobic respiration in an Arctic peat soil. *J Geophys Res* 2010;**115**:1–13.

Lipson DA, Raab TK, Goria D *et al.* The contribution of Fe(III) and humic acid reduction to ecosystem respiration in drained thaw lake basins of the Arctic Coastal Plain. *Global Biogeochem Cycles* 2013;**27**:399–409.

Lovley DR, Phillips EJP. Organic-matter mineralization with reduction of ferric iron in anaerobic sediments. *Appl Environ Microbiol* 1986;**51**:683–9.

Magen C, Lapham LL, Pohlman JW *et al.* A simple headspace equilibration method for measuring dissolved methane. *Limnol Oceanogr: Methods* 2014;**12**:637–50.

Malard LA, Anwar MZ, Jacobsen CS *et al.* Biogeographical patterns in soil bacterial communities across the Arctic region. *FEMS Microbiol Ecol* 2019;**95**:1–13.

Malard LA, Pearce DA. Microbial diversity and biogeography in Arctic soils. *Environm Microbiol Rep* 2018;**10**:611–25.

Megonigal JP, Hines ME, Visscher PT. Anaerobic metabolism: linkages to trace gases and aerobic processes. In: Holland HD, Turekian KK (eds), *Treatise on Geochemistry*. Vol **10**. Second. Amsterdam: Elsevier, 2014;273–359.

Methé ABA, Nelson KE, Eisen JA *et al.* Genome of *geobacter sulfurreducens*: metal reduction in subsurface environments. *Science* 2003;**302**:1967–9.

Miller KE, Lai CT, Friedman ES *et al.* Methane suppression by iron and humic acids in soils of the Arctic Coastal Plain. *Soil Biol Biochem* 2015;**83**:176–83.

Moosavi SC, Crill PM. CH4 oxidation by tundra wetlands as measured by a selective inhibitor technique. *J Geophys Res: Atmo* 1998;**103**:29093–106.

Myhre G, Shindell D, Bréon F-M *et al.* (eds.), *Climate Change2013: The Physical Science Basis. Contribution of Working Group I to the Fifth Assessment Report of the Intergovernmental Panel on Climate Change*. Cambridge, United Kingdom: Oxford University Press, 2013.

Neilson BT, Cardenas MB, O'Connor MT *et al.* Groundwater flow and exchange across the land surface explain carbon export patterns in continuous permafrost watersheds. *Geophys Res Lett* 2018;**45**:7596–605.

O'Connor MT, Cardenas MB, Neilson BT *et al. Active Layer Groundwater Flow: The Interrelated Effects of Stratigraphy, Thaw, and Topography*. 2019;**55**:6555–76.

Oksanen J, Blanchet FG, Kindt P *et al.* Vegan: community Ecology package. *R Package* 2013. **2.0-10**.

Parada AE, Needham DM, Fuhrman JA. Every base matters: assessing small subunit rRNA primers for marine microbiomes with mock communities, time series and global field samples. *Environ Microbiol* 2016;**18**:1403–14.

Patzner MS, Logan M, McKenna AM *et al.* Microbial iron cycling during palsa hillslope collapse promotes greenhouse gas emissions before complete permafrost thaw. *Commun Earth Environ* 2022; **3**:76

Philben M, Zhang L, Yang Z *et al.* Anaerobic respiration pathways and response to increased substrate availability of Arctic wetland soils. *Environ Sci: Proces Imp* 2020;**22**:2070–83.

Porsch K, Kappler A. FeII oxidation by molecular O_2 during hcl extraction. *Environ Chem* 2011;**8**:190–7.

Postma D, Jakobsen R. Redox zonation: equilibrium constraints on the Fe(III)/SO_4-reduction interface. *Geochim Cosmochim Acta* 1996;**60**:3169–75.

Quast C, Pruesse E, Yilmaz P *et al.* The SILVA ribosomal RNA gene database project: improved data processing and web-based tools. *Nucleic Acids Res* 2013;**41**:590–6.

R Core Teams. R: a language and environment for statistical computing. 2020.

Roberts D. labdsv: ordination and multivariate analysis for ecology. 2007.

Roden EE, McBeth JM, Blöthe M *et al.* The microbial ferrous wheel in a neutral pH groundwater seep. *Front Microbiol* 2012;**3**:1–18.

Roden EE, Wetzel RG. Organic carbon oxidation and suppression of methane production by microbial Fe(III) oxide reduction in vegetated and unvegetated freshwater wetland sediments. *Limnol Oceanogr* 1996;**41**:1733–48.

Rognes T, Flouri T, Nichols B *et al.* VSEARCH: a versatile open source tool for metagenomics. *PeerJ* 2016;**2016**:1–22.

Schloss PD, Westcott SL, Ryabin T *et al.* Introducing mothur: open-source, platform-independent, community-supported software for describing and comparing microbial communities. *Appl Environ Microbiol* 2009;**75**:7537–41.

Scott JJ, Breier JA, Luther GW *et al.* Microbial iron mats at the mid-atlantic ridge and evidence that zetaproteobacteria may be restricted to iron-oxidizing marine systems. *PLoS One* 2015;**10**: 1–19.

Shaver GR, Laundre JA, Bret-Harte MS *et al.* Terrestrial ecosystems at Toolik Lake, Alaska. In: Hobbie JE, Kling GW (eds), *Alaska's Changing Arctic: Ecological Consequences for Tundra, Streams and Lakes*. First. New York: Oxford University Press, 2014,352.

Sobolev D, Roden EE. Evidence for rapid microscale bacterial redox cycling of iron in circumneutral environments. *Antonie Van Leeuwenhoek* 2002;**81**:587–97.

Stookey LL. Ferrozine - a new spectrophotometric reagent for iron. *Anal Chem* 1970;**42**:779–81.

Vigliaturo R, Marengo A, Bittarello E *et al.* Micro- and nano-scale mineralogical characterization of Fe(II)-oxidizing bacterial stalks. *Geobiology* 2020;**18**:606–18.

Wagner R, Zona D, Oechel W *et al.* Microbial community structure and soil pH correspond to methane production in Arctic Alaska soils. *Environ Microbiol* 2017;**19**:3398–410.

Walker DA, Binnian E, Evans BM *et al.* Terrain, vegetation, and landscape evolution of the R4D research site, Brooks Range Foothills, Alaska. *Holoarctic Ecology* 1989;**12**:238–61.

Whalen SC, Cornwell JC. Nitrogen, phosphorus, and organic carbon cycling in an Arctic lake. *Can J Fish AquatSci* 1985;**42**:797–808.

Wickham H, Averick M, Bryan J *et al.* Welcome to the Tidyverse. *J Open Source Software* 2019;**4**:1686.

Zak DR, Kling GW. Microbial community composition and function across an Arctic Tundra landscape. *Ecology* 2006;**87**:1659–70.

Zhang S, Wang S, Shan X quan. Effect of sample pretreatment upon the metal speciation in sediments by a sequential extraction procedure. *Chem Spec Bioavailab* 2001;**13**:69–74.

Zhuang K, Izallalen M, Mouser P *et al.* Genome-scale dynamic modeling of the competition between Rhodoferax and Geobacter in anoxic subsurface environments. *ISME J* 2011;**5**:305–16.